MIT Libraries | DSpace@MIT

MIT Open Access Articles

A sub-terahertz broadband detector based on a GaN high-electron-mobility transistor with nanoantennas

The MIT Faculty has made this article openly available. ***Please share*** how this access benefits you. Your story matters.

Massachusetts Institute of Technology

IOPscience

A sub-terahertz broadband detector based on a GaN high-electron-mobility transistor with nanoantennas

You may also be interested in:

Plasma wave oscillations in nanometer field effect transistors for terahertz detection andemission
W Knap, F Teppe, N Dyakonova et al.

Photoresponse enhancement of plasmonic terahertz wave detector based on asymmetric silicon MOSFETs with antenna integration
Min Woo Ryu, Jeong Seop Lee, Kibog Park et al.

Characterization of a room temperature terahertz detector based on a GaN/AlGaN HEMT
Zhou Yu, Sun Jiandong, Sun Yunfei et al.

Enhancement of terahertz coupling efficiency by improved antenna design in GaN/AlGaN high electron mobility transistor detectors
Sun Yun-Fei, Sun Jan-Dong, Zhang Xiao-Yu et al.

Normally-off AlGaN/GaN high-electron-mobility transistor on Si(111) by recessed gate and fluorine plasma treatment
Jyun-Hao Lin, Shyh-Jer Huang, Chao-Hsing Lai et al.

High Johnson's figure of merit (8.32 THz·V) in 0.15-μm conventional T-gate AlGaN/GaN HEMTs on silicon
Kumud Ranjan, Subramaniam Arulkumaran, Geok Ing Ng et al.

Strained-Si modulation doped FETs as detectors of terahertz and sub-terahertz radiation
S L Rumyantsev, K Fobelets, D Veksler et al.

Nanometer size field effect transistors for terahertz detectors
W Knap, S Rumyantsev, M S Vitiello et al.

A sub-terahertz broadband detector based on a GaN high-electron-mobility transistor with nanoantennas

Haowen Hou[1,2], Zhihong Liu[1], Jinghua Teng[3], Tomás Palacios[4], and Soo-Jin Chua[1,2*]

[1]*Low-Energy Electronic System IRG, Singapore–MIT Alliance for Research and Technology Center, Singapore 138602*
[2]*Department of Electrical and Computer Engineering, National University of Singapore, Singapore 11758*
[3]*Institute of Materials Research and Engineering, Agency for Science, Technology, and Research (A*STAR), Singapore 138634*
[4]*Department of Electrical Engineering and Computer Science, Massachusetts Institute of Technology, Cambridge, MA 02139, U.S.A.*

*E-mail: elecsj@nus.edu.sg

We report a sub-terahertz (THz) detector based on a 0.25-µm-gate-length AlGaN/GaN high-electron-mobility transistor (HEMT) on a Si substrate with nanoantennas. The fabricated device shows excellent performance with a maximum responsivity (R_v) of 15 kV/W and a minimal noise equivalent power (NEP) of 0.58 pW/Hz$^{0.5}$ for 0.14 THz radiation at room temperature. We consider these excellent results as due to the design of asymmetric nanoantennas. From simulation, we show that indeed such nanoantennas can effectively enhance the local electric field induced by sub-THz radiation and thereby improve the detection response. The excellent results indicate that GaN HEMTs with nanoantennas are future competitive detectors for sub-THz and THz imaging applications. © 2017 The Japan Society of Applied Physics

In recent years, much attention has been focused on the research and development of electronic devices operating in the sub-terahertz (sub-THz) and THz regimes.[1] THz detectors based on Si metal–oxide–semiconductor field-effect transistors (MOSFETs)[2,3] and GaAs and InP high-electron-mobility transistors (HEMTs) have been widely reported.[4] The nonlinearity in the two-dimensional electron gas (2DEG) channel of a transistor has been proposed for broadband nonresonant detection from millimeter-wave radiation to THz radiation, with the advantages of room-temperature operation, high responsivity, and low equivalent noise power (NEP).[5] Compared with Si- and GaAs-based transistors, GaN-based HEMTs have a higher 2DEG channel density owing to the strong spontaneous piezoelectric polarization, large saturation velocity, high breakdown voltage, and ability to operate at high temperatures. GaN HEMTs are therefore one of the most promising devices for high-frequency, high-power, and high-temperature applications. Although GaN HEMTs for microwave communication and power applications are now commercially available,[6] there are only a few publications of GaN HEMTs working as detectors in THz and sub-THz ranges. Nonresonant detection in GaN HEMTs was first demonstrated by Knap et al. at 200 GHz.[5] Panasonic Corporation reported a detection responsivity of 1.1 kV/W at 1 THz using a GaN HEMT with 80 nm gate dipole antennas.[7] The detection of 0.9 THz radiation with 3.6 kV/W responsivity and 40 pW/Hz$^{0.5}$ NEP was also achieved in GaN HEMTs using floating antennas by Sun et al.[8]

An asymmetric antenna structure has been proposed to enhance the THz detector performance of InP HEMTs.[9,10] It has been reported that such an asymmetric antenna structure can enhance the detection responsivity by more than two orders compared with a symmetric structure.[10] In addition, a nanoantenna has also been proposed to enhance the electric field of THz radiation.[11–13] However, such a nanoantenna has not yet been reported to be applied in a HEMT THz detector. In this work, we demonstrated a GaN HEMT THz detector with asymmetric nanoantennas.

A simulation was carried out using COMSOL multiphysics to analyze the effect of nanoantennas on the electric field distribution in a HEMT detector under THz radiation. A GaN HEMT structure with a gate length of 250 nm was used in the simulation. A plane wave at 0.14 THz was used to illuminate the structure. The magnitude of the E-field of the incident THz plane wave was kept at 1 V/m. Figure 1 shows the simulated normalized electric field distribution on the GaN surface for two structures: (a) a novel HEMT with nanoantennas of 100 nm × 1 µm blocks uniformly distributed along the direction of the gate and a gap to the gate of 200 nm, and (b) a traditional HEMT without a nanoantenna array.

When THz radiation is coupled into the gate of the HEMT, a carrier density perturbation is induced in the 2DEG channel and decays exponentially with a distance of 30–300 nm from the source side of the gate edge to the drain side.[14] This means that the electric field at the gate edge of the device plays a significant role in the THz detection. As shown in Fig. 1(a), it can be seen that electric field intensity is greatly enhanced near the gate edge predominantly owing to the nanoantenna effect.[13] As the width of the electrodes is much smaller than the wavelength of the THz radiation, the electric field is strongly localized and confined. The introduction of nanoantennas effectively improves the localization of electric field owing to the strong carrier oscillation in the nanoscale metals. Figure 1(c) shows the electric field distribution along the cut line in Figs. 1(a) and 1(b). It can be seen from Fig. 1(c) that the nanoantenna-assisted evanescent wave tunnels through the subwavelength gap and couples into the gate electrode, which effectively improves the electric field intensity near the gate edge. Figure 1(d) shows a plot of the electric field intensity enhancement factor $|E_{nano}|^2/|E_{non\text{-}nano}|^2$ (defined as the ratio of the electric field intensity at the gate edge with nanoantennas to that at the gate edge without nanoantennas) as a function of the gap between the nanoantenna and the gate edge. It was found that the enhancement can be 2-fold in a 200 nm gap and up to 8-fold if the gap is shrunk to 50 nm. A similar strong terahertz near-field enhancement was also observed by Seo et al.[12]

The GaN HEMT fabricated in this work has epilayers including a 3 nm unintentionally doped (UID) GaN cap layer, a 20 nm UID Al$_{0.25}$Ga$_{0.75}$N barrier, a 1 nm AlN spacer, and a

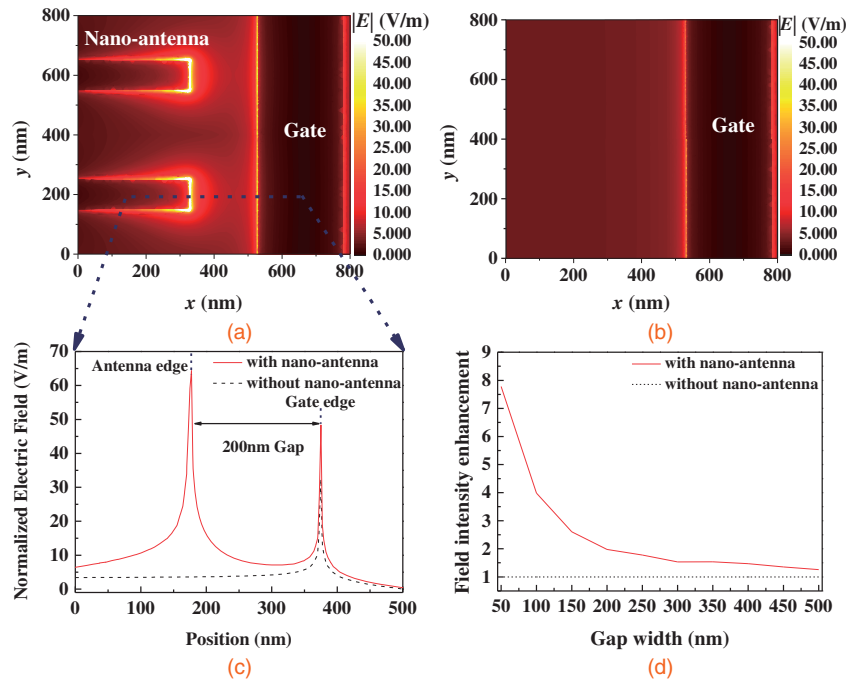© 2017 The Japan Society of Applied Physics

Fig. 1. Normalized distribution of the electric field $|E|$ on the GaN surface around the gate (top view) (a) with and (b) without nanoantennas. (c) Comparison of the electric field distributions along the cut lines in (a) and (b). (d) Field intensity enhancement as a function of the gap between the nanoantenna and the gate edge.
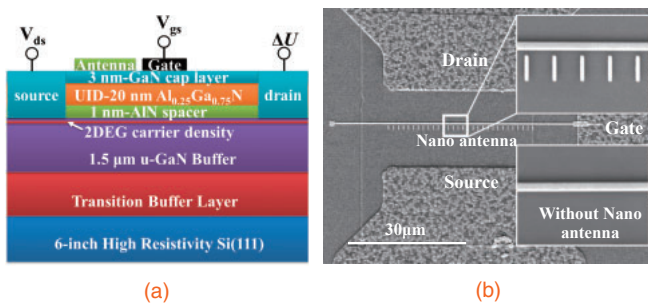

Fig. 2. (a) Schematic of the cross section and (b) SEM image of the top view of the GaN HEMT sub-THz detector. Inset figure: the device with the same dimensions but without a nanoantenna structure.

Fig. 3. Experimental setup for the sub-THz detector characterization.

1.5 µm UID GaN buffer, and was grown on a 6-in. high-resistivity Si(111) substrate with a thickness of 675 µm by metal organic vapor phase epitaxy. A schematic diagram of the cross section of the device is shown in Fig. 2(a). The 2DEG electron mobility and density characterized by Hall measurement are ~2100 cm^2 V^{-1} s^{-1} and ~1.0×10^{13} cm^{-2}, respectively. The device fabrication started with mesa isolation by BCl$_3$/Cl$_2$ plasma etching. Source and drain ohmic contacts were formed by Ti/Al/Ni/Au (20/120/40/50 nm) e-beam deposition followed by 850 °C rapid thermal annealing in N$_2$ ambient. The gate and nanoantennas were made of Ni/Au (20/80 nm) using e-beam lithography and lift-off processes. A scanning electron microscopy (SEM) image of the top view of the fabricated GaN HEMT sub-THz detector with nanoantennas is shown in Fig. 2(b). An asymmetric nanoantenna was placed near the gate of the HEMT. The gate length is 250 nm and the nanoantenna has dimensions of 100 nm × 1 µm. The gap between the gate and the nano-antenna is 200 nm. The source–drain distance is 14 µm and the mesa width is 35 µm.
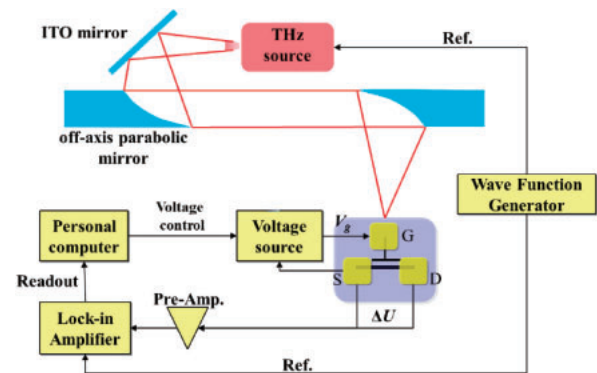
A schematic illustration of the high-frequency character-ization setup is shown in Fig. 3. A continuous-wave (CW) 0.14 THz sub-THz radiation was generated from an IMPATT diode and focused onto the surface of the GaN HEMT with nanoantennas by one indium tin oxide (ITO) mirror and two off-axis parabolic mirrors. A light-emitting diode (LED) was used to assist the alignment between the sub-THz radiation and the device. The radiation power focused onto the device area was calibrated using a standard pyroelectric power meter with an aperture of 1.5 mm diameter. The GaN HEMT was mounted on a FR-4 PCB board and its gate electrode was connected to a DC bias (GWInstek GPD-3303S). The source electrode of the GaN HEMT was grounded and the radiation-induced DC drain voltage (ΔU) was measured using a lock-in amplifier (Standford SR830). The sub-THz radiation source was modulated at 1111 Hz by a wave function generator, and the modulation signal was fed into the lock-in amplifier simultaneously. The DC electrical performance of the GaN HEMT was measured using a HP 4156A semi-conductor analyzer.
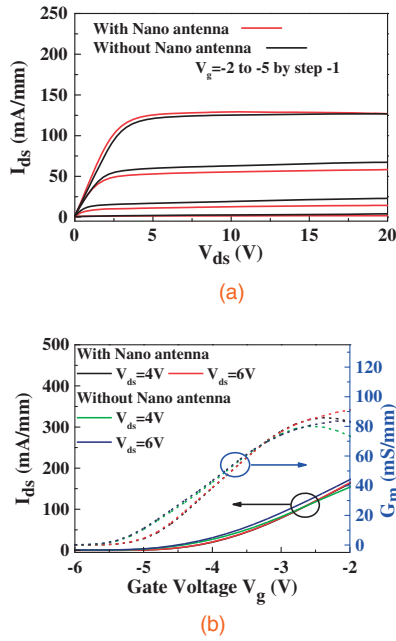
Fig. 4. DC (a) output and (b) transfer characteristics of the GaN HEMTs with and without nanoantennas.

Fig. 5. (a) Detection responsivity R_v values with and without nanoantennas. (b) NEP values measured at different gate voltages for the GaN HEMTs with and without nanoantennas at 0.14 THz radiation.

The DC output and transfer characteristics of the GaN HEMTs with and without nanoantennas are shown in Fig. 4. Both of the fabricated GaN HEMTs exhibited good gate modulation and similar transfer properties. The threshold voltage V_{th} is around -4.5 V for both devices. The device with nanoantennas has a slightly higher drain current I_{ds} and a higher transcendence g_m, which can be attributed to the nonuniformity across the whole 6-in. wafer.

Sub-THz detection was carried out at room temperature using the fabricated GaN HEMTs with and without nano-antennas. As shown in a previous work by Veksler et al.,[15] the drain current stimulates the THz response. In order to avoid the influence of drain bias, zero drain bias detection was performed for THz response measurement. In order to avoid the influence of bonding wires,[16] we ensure that bonding wires and the angles of incident THz waves are fully the same for the devices with and without nanoantennas. The responsivity R_v as a function of the gate voltage V_g is plotted in Fig. 5. The responsivity R_v is defined as $\Delta U/P_d$, where ΔU is the measured photovoltage and P_d is the radiation power on the detector. Assuming that the radiation power is uniformly distributed over the beam spot size, P_d can be estimated as $P_d = P_b \cdot (A_d/A_b)$, where P_b is the total power of the beam, A_b is the beam spot size, and A_d is the active area of the detector. The procedure used to determine P_d can be found in other reports.[4] We estimate our active area following the method in Ref. 4 using active mesa dimensions of $14 \times 35 \, \mu m^2$ and total dimensions of one pixel of $324 \times 230 \, \mu m^2$.

As can be seen in Fig. 5, the maximum responsivity of the GaN HEMT for the radiation at 0.14 THz is 15 kV/W at room temperature, which is among the best values reported for nonresonant detection by GaN HEMTs.[7,8] Figure 6 shows the reported best THz detector performance based on various semiconductor transistors. For comparison, the device without nanoantennas has a responsivity of around 8.3 kV/W, which is an approximately 1.8-fold enhancement for the device with nanoantennas. In a general picture, the detector's output
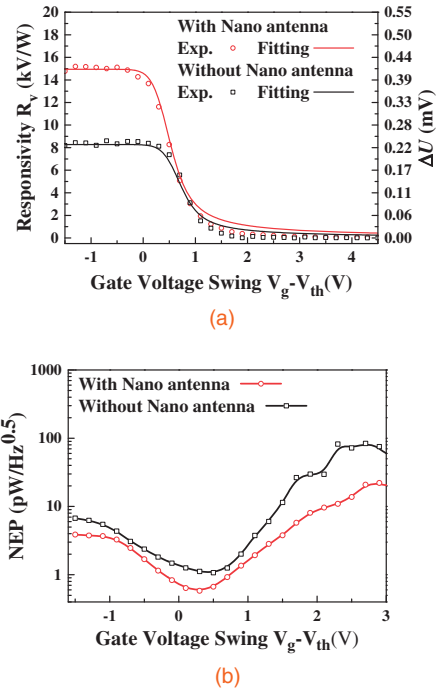
voltage $\Delta U \propto eU_a^2/4\eta k_B T$,[5] where U_a is the amplitude of the gate-to-source voltage induced by incident THz radiation, e is the electron charge, η is the subthreshold slope, k_B is the Boltzmann constant, and T is the absolute temperature. The term $e/k_B T$ is constant at room temperature. The subthreshold slope η can be determined by the transconductance g_m as shown in Fig. 4(b). By theoretical fitting[17] as shown in Fig. 5(a), U_a^2 is found to be $1.95 \times 10^{-4} \, V^2$ for the device with nanoantennas and $1.08 \times 10^{-4} \, V^2$ for the device without nanoantennas. The term U_a depends on the power of the THz source and the coupling efficiency between the incident radiation and the gate diode in the HEMT. As shown by the above simulation, owing to the nanoantennas located near the gate, a strong localization field was induced and the THz radiation was more efficiently coupled to the 2DEG channel, leading to an enhancement of U_a. Thus, the output voltage ΔU and therefore the responsivity R_v are improved. The silicon substrate has a significant influence on the detector perform-ance,[18] and the performance of our device can be expected to be higher if the substrate is thinned down below 100 μm.

Moreover, the responsivity versus the gate voltage swing $V_g - V_{th}$ has a sigmoidlike behavior. When $V_g > V_{th}$, the responsivity is very small and only around 50 V/W. When V_g shifts negatively and closer to V_{th} (-4.5 V), the responsivity begins to rise rapidly and reaches a plateau after the device 2DEG channel is considerably depleted ($V_g < V_{th}$). The sub-THz responsivity remains constant all the way to $V_g = -6$ V. The GaN device measured here has a relatively low channel resistance ($R_{ch} \sim 200 \, k\Omega$) owing to the large gate leakage when V_g is below the threshold voltage, which is much smaller than the input impedance of the lock-in amplifier ($Z_{in} = 10 \, M\Omega$). Therefore, the loading effect, which causes the responsivity drop after $V_g < V_{th}$ observed during the measurement using a lock-in amplifier,[17,19] is negligible for our GaN HEMT terahertz detector.
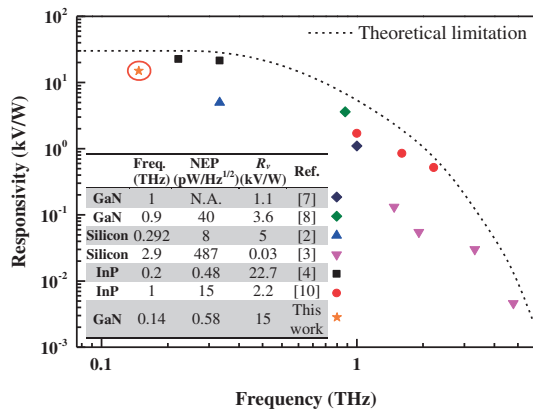
Fig. 6. Summary of the reported THz detection performance characteristics of different HEMTs at room temperature. The dashed line shows a theoretical curve for responsivity limitation.[3]

Fig. 7. GaN HEMT responsivity to 0.14 THz radiation versus the polarization angle.

NEP is an important parameter used to evaluate the detector performance. The dominant noise source in the GaN HEMT detector is the thermal noise from the GaN channel. Therefore, the NEP can be estimated as $NEP = (4kTR_{ds})^{0.5}/R_v$, where R_{ds} is the channel resistance and R_v is the detector responsivity.[2] R_{ds} can be determined from the static transfer characteristics shown in Fig. 4(b). Figure 5(b) shows the NEP values as a function of gate voltage. A minimal NEP value of 0.58 pW/Hz$^{0.5}$ is achieved at $V_g = -4.2$ V at room temperature. In comparison, the device without nanoantennas has a minimal NEP of 1.07 pW/Hz$^{0.5}$. This NEP improvement can be attributed to the responsivity enhancement from nanoantennas. When V_g becomes negative, the NEP decreases for V_g first owing to the increase in responsivity and then increases for V_g below -4.2 V owing to the increase in output channel resistance. The NEP for our nanoantenna device is comparable to other reports of the FET-based detection of sub-THz waves[2,4] as shown in the inset table in Fig. 6.

It is worthy to note that, although the gate leakage current suppresses the loading effect and minimizes the responsivity drop when $V_g < V_{th}$ during the measurement using a lock-in amplifier, it would not increase the device's intrinsic responsivity. It is still desired to improve the device's gate structure design, for example, by adopting a MOS structure to reduce the gate leakage current, because a large gate leakage current will introduce extra shot noise, increase the NEP, and also result in long-term reliability issues.

The nonresonant detection in a GaN HEMT is typically sensitive to the polarization of the incident electromagnetic (EM) wave. Figure 7 shows the polarization dependence of the response with different azimuthal angle φ values between the incident EM electric field and the HEMT source-to-drain direction. The maximum response was obtained at $\varphi = 0$, where the incident field is parallel to the source–drain direction. A two-lobe shape for the responsivity is observed, which follows well the $\cos^2\varphi$ law. The discrepancy of the size of one lobe from the theory is due to the influence of the bonding wire interacting with the incident beam.[16]

In conclusion, room-temperature sub-THz detection by AlGaN/GaN HEMTs with novel nanoantennas was demonstrated. A maximum responsivity above 15 kV/W and a minimum NEP of 0.58 pW/Hz$^{0.5}$ for 0.14 THz radiati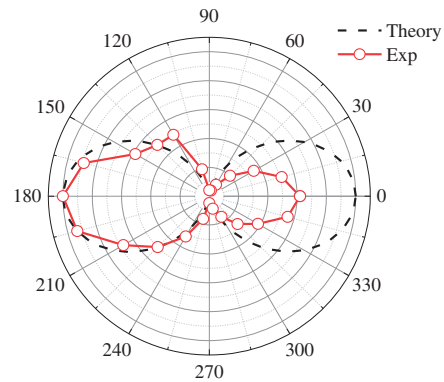on were obtained. The response was found to be polarization-dependent. The promising results indicate the great potential for GaN HEMTs to be used as sub-THz detectors for various applications.

1) M. Tonouchi, Nat. Photonics **1**, 97 (2007).
2) F. Schuster, D. Coquillat, H. Videlier, M. Sakowicz, F. Teppe, L. Dussopt, B. Giffard, T. Skotnicki, and W. Knap, Opt. Express **19**, 7827 (2011).
3) S. Boppel, A. Lisauskas, M. Mundt, D. Seliuta, L. Minkevicius, I. Kasalynas, G. Valusis, M. Mittendorff, S. Winnerl, V. Krozer, and H. G. Roskos, IEEE Trans. Microwave Theory Tech. **60**, 3834 (2012).
4) Y. Kurita, G. Ducournau, D. Coquillat, A. Satou, K. Kobayashi, S. Boubanga Tombet, Y. M. Meziani, V. V. Popov, W. Knap, T. Suemitsu, and T. Otsuji, Appl. Phys. Lett. **104**, 251114 (2014).
5) W. Knap, V. Kachorovskii, Y. Deng, S. Rumyantsev, J.-Q. Lü, R. Gaska, M. S. Shur, G. Simin, X. Hu, M. A. Khan, C. A. Saylor, and L. C. Brunel, J. Appl. Phys. **91**, 9346 (2002).
6) S. T. Sheppard, K. Doverspike, W. L. Pribble, S. T. Allen, J. W. Palmour, L. T. Kehias, and T. J. Jenkins, IEEE Electron Device Lett. **20**, 161 (1999).
7) T. Tanigawa, T. Onishi, S. Takigawa, and T. Otsuji, Device Research Conf. (DRC), 2010, p. 167.
8) J. D. Sun, Y. F. Sun, D. M. Wu, Y. Cai, H. Qin, and B. S. Zhang, Appl. Phys. Lett. **100**, 013506 (2012).
9) V. V. Popov, D. V. Fateev, T. Otsuji, Y. M. Meziani, D. Coquillat, and W. Knap, Appl. Phys. Lett. **99**, 243504 (2011).
10) T. Watanabe, S. B. Tombet, Y. Tanimoto, Y. Wang, H. Minamide, H. Ito, D. Fateev, V. Popov, D. Coquillat, W. Knap, Y. Meziani, and T. Otsuji, Solid-State Electron. **78**, 109 (2012).
11) P. Mühlschlegel, H.-J. Eisler, O. J. F. Martin, B. Hecht, and D. W. Pohl, Science **308**, 1607 (2005).
12) M. A. Seo, H. R. Park, S. M. Koo, D. J. Park, J. H. Kang, O. K. Suwal, S. S. Choi, P. C. M. Planken, G. S. Park, N. K. Park, Q. H. Park, and D. S. Kim, Nat. Photonics **3**, 152 (2009).
13) H. Tanoto, J. H. Teng, Q. Y. Wu, M. Sun, Z. N. Chen, S. A. Maier, B. Wang, C. C. Chum, G. Y. Si, A. J. Danner, and S. J. Chua, Sci. Rep. **3**, 2824 (2013).
14) W. Knap, S. Rumyantsev, M. S. Vitiello, D. Coquillat, S. Blin, N. Dyakonova, M. Shur, F. Teppe, A. Tredicucci, and T. Nagatsuma, Nanotechnology **24**, 214002 (2013).
15) D. Veksler, F. Teppe, A. P. Dmitriev, V. Y. Kachorovskii, W. Knap, and M. S. Shur, Phys. Rev. B **73**, 125328 (2006).
16) M. Sakowicz, J. Łusakowski, K. Karpierz, M. Grynberg, W. Knap, and W. Gwarek, J. Appl. Phys. **104**, 024519 (2008).
17) M. Sakowicz, M. B. Lifshits, O. A. Klimenko, F. Schuster, D. Coquillat, F. Teppe, and W. Knap, J. Appl. Phys. **110**, 054512 (2011).
18) D. Coquillat, J. Marczewski, P. Kopyt, N. Dyakonova, B. Giffard, and W. Knap, Opt. Express **24**, 272 (2016).
19) W. Stillman, M. S. Shur, D. Veksler, S. Rumyantsev, and F. Guarin, Electron. Lett. **43**, 422 (2007).